Local environment of optically active Nd^{3+} ions in the ultratransparent $BaMgF_4$ ferroelectric crystal

J. E. Muñoz-Santiuste,[1] H. Loro,[2] R. Marino,[3] Ph. Goldner,[3] V. Vasyliev,[4] E. G. Víllora,[4] K. Shimamura,[4] P. Molina,[5,*] M. O. Ramírez,[5] and L. E. Bausá[5]

[1]*Dpto. de Física, Escuela Politécnica Superior, Universidad Carlos III de Madrid, Leganes, 28911 Madrid, Spain*

[2]*Facultad de Ciencias, Universidad Nacional de Ingeniería, P.O. Box 31-139, Lima, Perú*

[3]*Laboratoire de Chimie de la Matière Condensée de Paris, Chimie-Paristech, CNRS UMR 7574, UPMC Univ. Paris 06, 11, rue Pierre et Marie Curie, F-75005 Paris, France*

[4]*National Institute for Materials Science, 1-1 Namiki, Tsukuba 305-0044, Japan*

[5]*Dpto. Física de Materiales and Instituto Nicolás Cabrera, Universidad Autónoma de Madrid, 28049-Madrid, Spain*

(Received 30 March 2012; published 24 May 2012)

A comprehensive study of the site location of Nd^{3+} ions in the $BaMgF_4$ ultratransparent ferroelectric crystal is presented. By combining different low-temperature optical spectroscopies and electron paramagnetic resonance, the crystal field energy levels of Nd^{3+} ions and the gyromagnetic factors are experimentally determined. These results are employed to perform the crystal field analysis of Nd^{3+} ions considering a Cs point symmetry. The crystal field calculation yields a small root-mean-square deviation of 18 cm^{-1} and reveals a large crystal field strength (621 cm^{-1}), verifying the assignment of the Ba^{2+} cationic site as the location for Nd^{3+} ions in this fluoride host. The results suggest a slight displacement of Nd^{3+} from the barium regular site with a rearrangement of the fluorine ions around it. The work gives a deep insight into the properties of the Nd^{3+}-doped $BaMgF_4$ crystal, a ferroelectric widely ultra-transparent material with potential applications as optical device operating in the Vacuum Ultraviolet-Ultraviolet and midinfrared spectral regions.

DOI: 10.1103/PhysRevB.85.184110 PACS number(s): 61.72.U−, 78.30.−j, 76.30.Kg, 71.55.−i

I. INTRODUCTION

Ferroelectrics are key systems for the development of a great number of relevant applications in different fields of technology. These materials have been playing an important role in photonic devices due to their suitable electro-optic and nonlinear properties for light control. They are successfully used as high-speed light modulators, parametric oscillators, or nonlinear frequency converters, covering a wide range of the optical spectrum.[1–4] Moreover, in the last years, it has been demonstrated that these materials can also operate as optically active systems generating laser action when the appropriate optical impurities are incorporated into the crystals.[5–7] In this context, the use of ferroelectric crystals as host matrices for optically active ions has emerged as an attractive field to develop multifunctional compact solid-state lasers with the added functions of self-multidirectional and self-multiwavelength frequency conversion, self-deflection of the coherent radiation, tunability, or even optical bistability.[8–10]

In this paper, we investigate the properties of Nd^{3+} ions in the $BaMgF_4$ crystal (hereafter BMF), the only ferroelectric fluoride crystal reported up to now.[11] BMF is a nonlinear crystal which exhibits an extraordinary transparency range extending from the deep ultraviolet (UV) (126 nm) to the midinfrared (IR) (13 μm).[12,13] This offers an exceptional advantage for optical devices operating in the UV and mid-IR, where other nonlinear materials cannot be used. Regarding its photonic applications, quasiphase-matched frequency conversion processes in both visible and UV spectral region have been recently reported in periodically poled BMF crystals being the shortest converted wavelength obtained in the UV at 368 nm.[14] In this crystal, the value of the coercive field is remarkably lower than those of stoichiometric or congruent $LiNbO_3$ and $LiTiO_3$ and the grating periods for quasiphase matching much larger,[15] which clearly facilitates the fabrication process of periodical structures of inverted domains.

BMF belongs to the pyroelectric fluoride $BaMeF_4$ family (Me = Mg, Mn, Fe, Co, Ni, Zn). It crystallizes in the orthorhombic system with space group $Cmc2_1$, and it has four molecules per unit cell. The orthorhombic structure of BMF indicates that it is optically biaxial, with the principal optical axes *xyz* coincident with the crystallographic ones *abc* in some order. Pure (undoped) BMF crystals were first grown back in the 1970s by both Bridgman and Czochralski techniques, and the main optical, elastic, and electric properties of BMF were reported.[12,16,17]

The crystal structure consists of distorted MgF_6 octahedra sharing corners to form puckered sheets parallel to (010) plane. These are linked by Ba^{2+} ions. Both cations Ba^{2+} and Mg^{2+} are located in a mirror plane parallel to the (100) plane, occupying a Wyckoff 4*a* site with a local symmetry C_s.[18] Figure 1(a) shows the projection of the BMF structure on the (100) plane containing the ferroelectric *c* axis. It displays the available cationic sites: (i) Mg^{2+} sites with C_s symmetry and sixfold coordination in an octahedral environment and (ii) Ba^{2+} sites with C_s symmetry and 11-fold coordination. Figure 1(b) shows a detail of the Ba^{2+} environment in the BMF lattice. It consists of six fluorine atoms at the apices of a trigonal prism, together with five more located equatorially through the rectangular faces of the prism on a plane parallel to the *bc* plane.

The incorporation of trivalent rare earth ions in this nonlinear host crystal has been the subject of some recent reports.[19–21] In particular, the possibility of incorporating Nd^{3+} ions has been recently demonstrated, opening the way to the development of potential self-frequency converted all solid-state lasers operating in the UV and vacuum-UV (VUV) and mid-IR spectral regions.[11] Namely, by means of site selective spectroscopy, it has been recently shown that Nd^{3+}

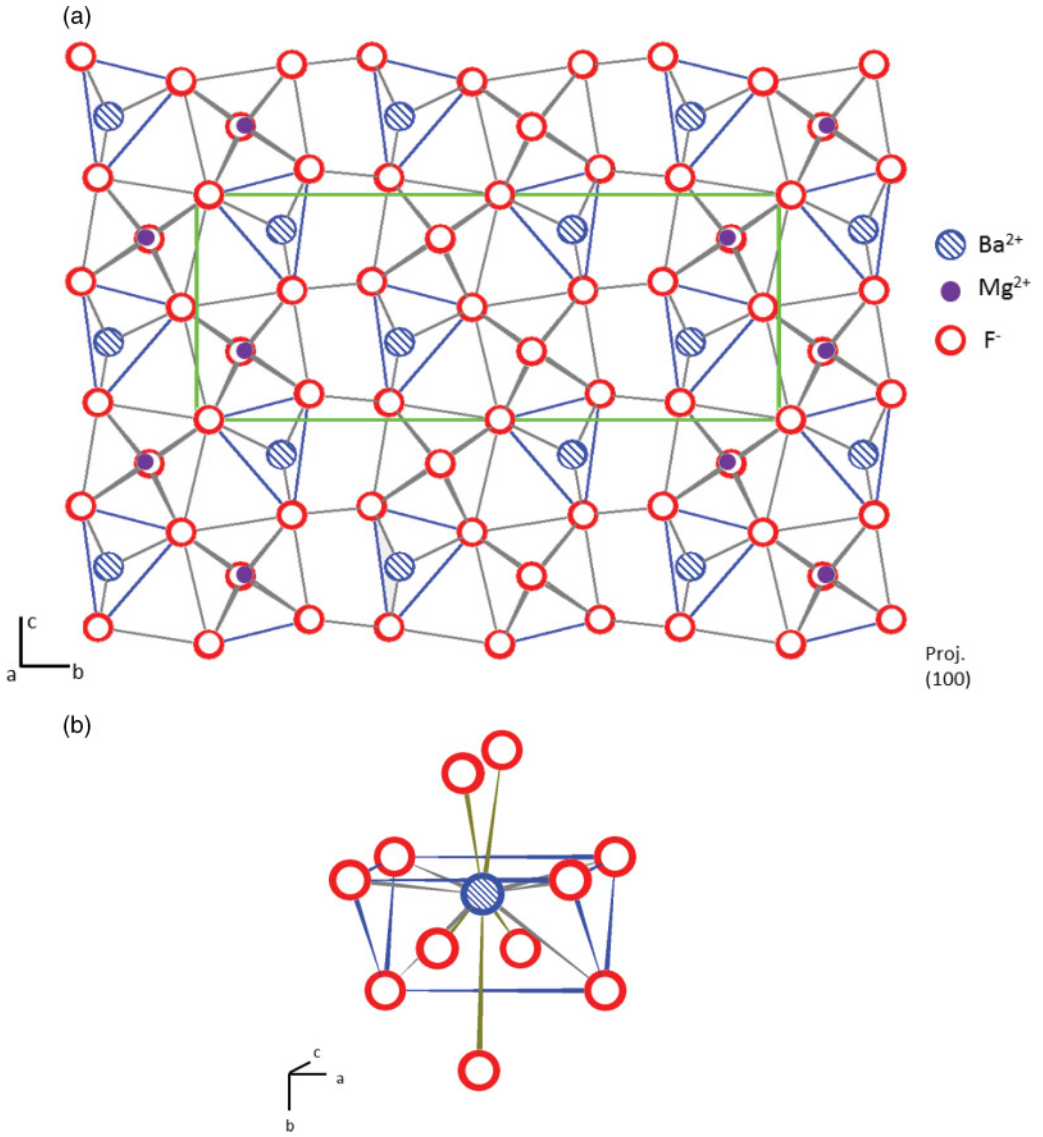

FIG. 1. (Color online) (a) Projection of the $BaMgF_4$ crystalline structure along the *a* axis. (b) Coordination of fluorine atoms around Ba^{2+}.

incorporates into the BMF matrix at two well-differentiated centers referred to as A (dominant) and B (minor) centers. As suggested, those two Nd^{3+} centers can be associated with Nd^{3+} in a Ba^{2+} regular lattice site (A center) and with a defect-distorted Ba^{2+} site (B center). The annihilation of the minor defect-distorted B center can be achieved by the incorporation of Na^{+} ions into the crystal. These ions provide the charge compensation mechanism required when Nd^{3+} ions substitute for a divalent cation in the lattice and prevent the presence of undesired defects in the lattice.[11] Additionally, as previously confirmed by site selective spectroscopy, the presence of Na^{+} ions does not affect the spectroscopic characteristics of the major center, which suggest that the charge compensation for the A major center is not local.

Due to the interest of Nd^{3+} as a laser active ion and that of the BMF as a widely ultratransparent nonlinear host, here, we present a detailed investigation to establish a model for the local environment of Nd^{3+} ions in BMF. The codoped BMF:Na^{+}:Nd^{3+} crystal has been chosen because of two reasons: (i) it shows a better crystal quality than the singly Nd^{3+}-doped BMF crystal and (ii) it displays a single Nd^{3+} center (A center), which facilitates the identification of the energy levels and the crystal field (CF) analysis. Different experimental techniques, specifically, low-temperature (LT) optical spectroscopy, Fourier-transform infrared spectroscopy (FTIR), and LT electron paramagnetic resonance (EPR), have been combined. The LT optical (absorption and emission) and FTIR spectra have been used to identify the greatest possible number of Stark energy levels, particularly those related to the ^4I_J $(J = 9/2, \ldots, 15/2)$ lowest multiplet. Electron paramagnetic resonance spectroscopy has been used to obtain Nd^{3+} ground state *g* factors, which are closely linked to wave functions and can be used to test further the crystal field (CF) calculations. This technique also gave information about the Nd^{3+} site symmetry. Then, a standard Hamiltonian, including free ion interactions and CF terms of C_s symmetry,

was used to fit the experimentally obtained energy levels of the Nd^{3+} ($4f^3$) configuration. Additionally, the principal g values corresponding to the lowest (0 cm^{-1}) energy level were estimated and compared with those obtained by the EPR technique.

II. EXPERIMENTAL DETAILS

A BMF single crystal, with an Nd^{3+} and Na^+ content of 0.02 and 0.15 mol% (referred to Ba^{2+}), was prepared by the Czochralski technique using a 30-kW RF generator. The low Nd^{3+} concentration clearly favors its presence as isolated ions in the crystal, which is advantageous in the context of this work. More details on the growth procedure can be found elsewhere.[13] From the boule, samples were cut with the c axis parallel or perpendicular to the main face in order to perform the optical measurements and the EPR experiments.

The optical absorption measurements were obtained from the UV to the IR spectral range by means of a Perking Elmer Lambda 1050 spectrophotometer. For the luminescence experiments, an Argon-pumped continuous wave tunable Ti:Sapphire laser (Spectra Physics 3900) was used as an excitation source. The emission was detected with a Peltier cooled charge coupled device camera or a Ge-detector. Low-temperature FTIR data were taken with a Perkin-Elmer 2000 Fourier-transform IR spectrometer. Low-temperature (nominal 10 K) optical absorption, emission, and FTIR spectra were obtained using a closed-cycled helium optical cryostat. All optical spectroscopy and FTIR experiments were performed with unpolarized light launching the proof beam parallel to the ferroelectric c axis of the crystal.

Electron paramagnetic resonance measurements were performed at 5 K with an X-band (9.5 GHz) Bruker ELEXSYS E 500 spectrometer, equipped with a variable-temperature accessory from Oxford Instrument. The crystals were mounted on a small Perspex sample holder to allow their orientation with respect to the magnetic field. The principal g values, namely g_x, g_y, and g_z, were determined from the angular variations of the experimental g factor in the three orthogonal crystallographic planes (ab), (bc), and (ac). These angular variations were obtained by rotating the crystal in 10° steps around the reference axes with ≈2° accuracy.

III. RESULTS AND DISCUSSION

A. Low temperature optical spectroscopy

In order to calculate the CF parameters of Nd^{3+} in BMF:Na host matrix, a total of 51 experimental CF energy levels arising from the $4f^3$ electronic configuration of the free Nd^{3+} ion were assigned in the optical spectra. For this purpose, a combination of LT linear absorption, fluorescence, and FTIR spectroscopy was used.

Special attention was paid to the Stark energy levels of the ^4I_J (J = 9/2, 11/2, 13/2, and 15/2) states of Nd^{3+} ions due to their relevance on the CF calculations for low-symmetry environments. The spectra involving those ^4I_J states are shown in Fig. 2. The LT emission spectra of Nd^{3+} in BMF:Na^+ associated with the $^4F_{3/2} \rightarrow {}^4I_{9/2}$, $^4F_{3/2} \rightarrow {}^4I_{11/2}$, and $^4F_{3/2} \rightarrow {}^4I_{13/2}$ transitions are displayed in Figs. 2(a)–2(c). The excitation energy was 11 764 cm^{-1} (850 nm), coinciding with the transition from the lowest Stark energy level of the $^4I_{9/2}$ ground state up to the highest excited level of the $^4F_{3/2}$ state. The emission spectra consist of five ($^4I_{9/2}$), six ($^4I_{11/2}$), and seven ($^4I_{13/2}$) lines in agreement with the expected CF splitting of the corresponding $^{2S+1}L_J$ states into (2J + 1)/2 Stark levels at C_s symmetry for a single Nd^{3+} center. Thus, by using 10 K optical fluorescence spectroscopy, the set of the Stark energy levels of the $^4I_{9/2}$, $^4I_{11/2}$, and $^4I_{13/2}$ can be obtained (see Table I). Low-temperature absorption and FTIR measurements in the 1900–6700 cm^{-1} energy range allow us to confirm the previous assignments as well as to identify five of the seven Stark energy levels of the $^4I_{15/2}$ excited state. Figure 2(d) shows the LT optical absorption spectrum in the 5700–6700 cm^{-1} energy range related to the $^4I_{9/2} \rightarrow {}^4I_{15/2}$ transition of Nd^{3+}. The data depicted on Figs. 2(e) and 2(f) correspond to the FTIR experiments collected at 10 K for the $^4I_{9/2} \rightarrow {}^4I_{11/2}$ and $^4I_{9/2} \rightarrow {}^4I_{13/2}$ optical transitions of Nd^{3+}, respectively. These measurements are complementary to those displayed in Figs. 2(b) and 2(c). In both cases the final state is the same, and so they confirm the energy positions of the different Stark sublevels. An excellent agreement on the energy levels assignment was found by using both spectroscopic techniques.

The Stark energy levels of the different ^4F_J (J = 5/2, 7/2, and 9/2) excited states have been also analyzed by means of the optical transitions from the lowest Stark energy level of the fundamental $^4I_{9/2}$ state. Figure 3 shows the corresponding LT absorption spectrum in the 12 350–15 350 cm^{-1} energy range. As expected, the spectrum consists of three groups of lines centered at around 12 650 ($^4F_{5/2}$), 13 700 ($^4F_{7/2}$), and 14 925 ($^4F_{9/2}$) cm^{-1}. The energy positions of the Stark components of the $^4F_{3/2}$ state have been obtained by means of the broad band excitation spectrum in the 11 500–11 900 cm^{-1} spectral region. The monitored wavelength was 1049 nm (9532 cm^{-1}). The spectrum is shown in the inset of Fig 3. Two well-resolved bands at 11 540 and 11 778 cm^{-1}, which correspond to the transitions from the lowest Stark level of the fundamental state $^4I_{9/2}(0)$ to the $^4F_{3/2}(1)$ and $^4F_{3/2}(2)$ excited Stark sublevels, are observed according to the expected CF splitting of the $^4F_{3/2}$ state. As in most of Nd^{3+}-doped compounds, the spectral shape of the $^4F_{3/2}(2)$ line exhibits a rather complicated structure, being much broader than the $^4F_{3/2}(1)$ one as a result of a fast nonradiative decay.

The LT optical absorption spectrum corresponding to more energetic transitions is shown in Fig. 4. It displays the transitions from the $^4I_{9/2}(0)$ ground level up to the different Stark levels of the ^4G_J, $^2P_{1/2}$, and ^4D_J excited states, as indicated in the figure. The inset depicts a detail of the $^4I_{9/2}(0) \rightarrow {}^2P_{1/2}$ transition. In agreement with the multiplicity of that state, a single and well-resolved line is observed, evidencing the presence of a single Nd^{3+} center, as previously reported on Nd^{3+} and Na^+-codoped BMF.[11] At this point, it is important to mention that previous studies have pointed out that trivalent lanthanide ions substitute for Ba^{2+} cations in the BMF crystal lattice.[19] This can be justified on the basis of the well-established set of ionic radii published by Shannon.[22] For the specific case of trivalent neodymium in coordination

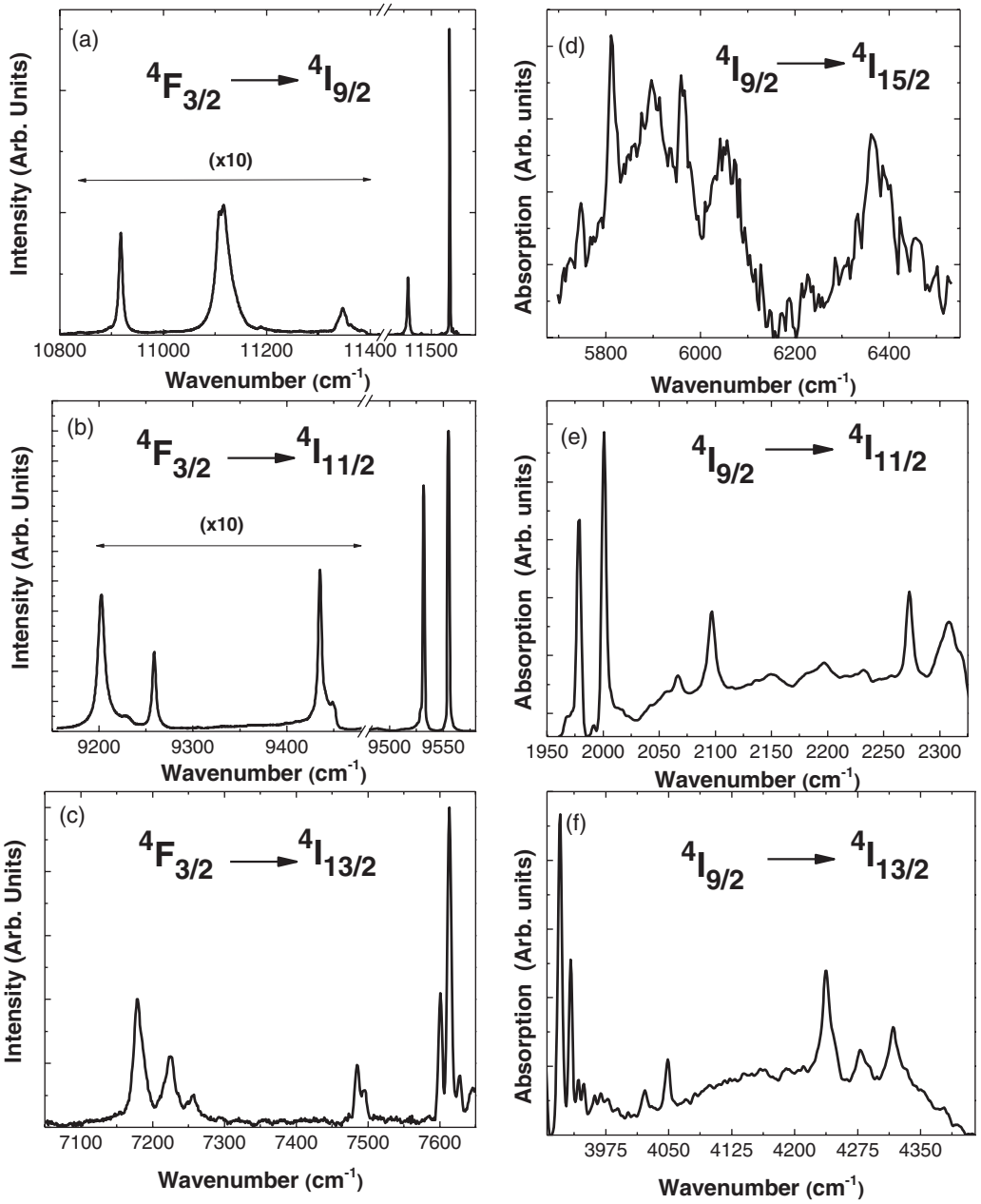

FIG. 2. Low-temperature (10 K) emission spectra of the Nd^{3+} ion in BMF:Na^+ crystal associated with the (a) $^4F_{3/2} \rightarrow {}^4I_{9/2}$, (b) $^4F_{3/2} \rightarrow {}^4I_{11/2}$, and (c) $^4F_{3/2} \rightarrow {}^4I_{13/2}$ transitions, respectively; LT IR absorption spectra from the $^4I_{9/2}$ ground level to the (d) $^4I_{15/2}$, (e) $^4I_{11/2}$, and (f) $^4I_{13/2}$ states.

number 6, the ionic radius is 130 pm, while the ionic radii of Ba^{2+} and Mg^{2+} are 156 and 86 pm, respectively. Nd^{3+} ion seems to be too large to be easily accommodated at the Mg^{2+} octahedral site in the BMF lattice, so size considerations further support the preferential location in Ba^{2+} site.

B. Electron paramagnetic resonance

Figure 5 shows the angular variations of the g^2 factor in the three crystallographic (ab), (bc), and (ac) planes. These variations were fitted with the expression:

$$g^2(\theta) = g_{ii}^2 \cos^2(\theta) + g_{jj}^2 \sin^2(\theta) \pm 2g_{ij}^2 \sin(\theta)\cos(\theta), \quad (1)$$

where i and j stand for the axis labels (a, b, or c), and θ is the angle for the i axis. Since the g^2 values are maximal along the a, b, and c axes, the g_{ij} factors are zero, and the g matrix is diagonal in the a, b, and c axes. This suggests that the Nd^{3+} site symmetry is close to orthorombic and is distorted from the site of Ba^{2+} ions. The g matrix values are $g_{aa} = g_x = 2.84 \pm 0.01$, $g_{bb} = g_y = 1.44 \pm 0.01$ and $g_{cc} = g_z = 2.99 \pm 0.01$. Figure 6(a) presents a typical spectrum when the field is in the (ac) plane. Apart from the strong Zeeman line, one can see the hyperfine structures corresponding to the two nonzero nuclear spin isotopes ($I = 7/2$) $^{145}Nd^{3+}$ and $^{143}Nd^{3+}$. In the (ab) and (bc) planes, two Zeeman lines appeared [Fig. 6(b)],

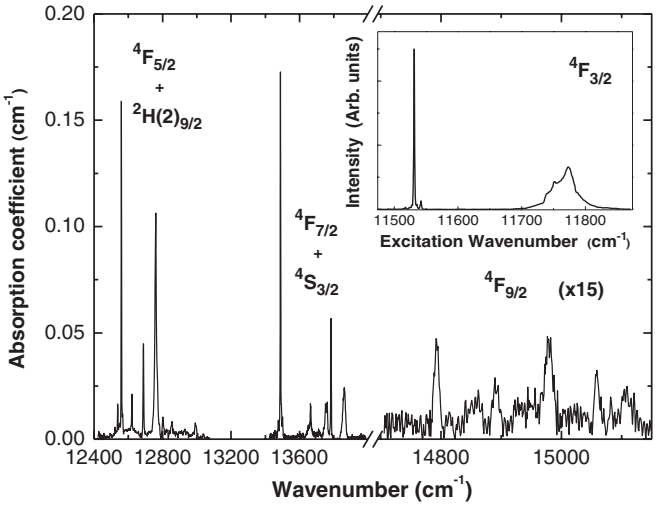

FIG. 3. Low-temperature absorption spectrum of Nd^{3+} ions in BMF:Na^+ from the $^4I_{9/2}$ ground state to the ^4F_J (J = 5/2, 7/2) excited states. The inset shows the excitation spectrum to the $^4F_{3/2}$ state monitoring the 1049-nm emission wavelength.

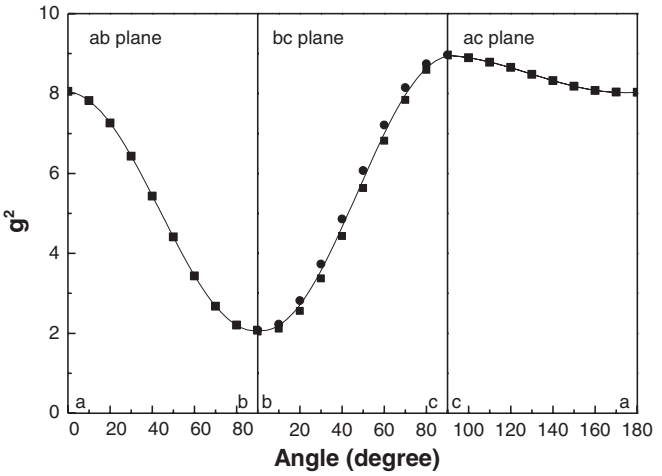

FIG. 5. Experimental and simulated angular variations of g^2 in the (ab), (bc), and (ac) planes. In the (bc) planes, variations of the two Zeeman lines are reported (see text).

with a larger splitting in the latter case. This can be explained with slightly magnetically nonequivalent sites related by a symmetry plane parallel to the (ac) plane, in agreement with the crystal structure.[19] The angular variations of the two lines in the (bc) plane are given on Fig. 5.

C. Crystal field calculations

To estimate the CF acting on the Nd^{3+} ions in the BMF:Na^+ crystal, the C_s CF parameters have been calculated. For this purpose, the energy levels obtained by the different spectroscopic techniques have been used. These experimental energy levels have been listed in Table I.

The optical properties and the energy levels of the lanthanides in solids are ruled by the interelectronic interaction between the electrons of the inner $4f$ shell of the lanthanide and the charge of the host ligands, all distributed in a particular local point symmetry. The complete Hamiltonian (free-ion plus CF interactions) describing the lanthanide ions in solids uses a parametric method, in which a small group of phenomenological parameters allow to reproduce the lanthanide energy level diagram. In the framework of the Racah algebra, these phenomenological parameters are numeric coefficients that multiply a tensor operator to describe the interaction. The adjustable parameters are radial integrals, while the angular components of the tensor operators can be calculated exactly with the help of the tensor algebra and the group theory.[23]

The free-ion Hamiltonian, that includes Slater–Condon, F^k, spin-orbit, ζ_{so}, two body interaction, α, β, and γ, Judd parameters T^i, spin-other-orbit parameters, M^j, and electrostatically correlated spin-orbit interaction parameters

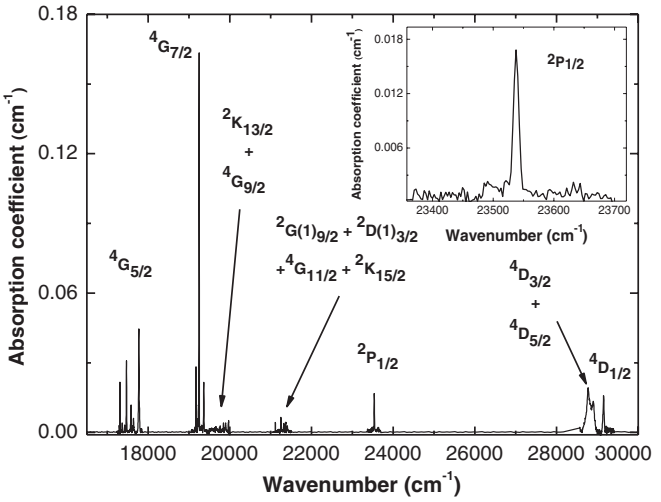

FIG. 4. Low-temperature absorption spectrum of Nd^{3+}-doped BMF:Na^+ showing the transitions from the $^4I_{9/2}(0)$ ground level to the ^4G_J, $^2P_{1/2}$, and ^4D_J excited states. The inset shows the single line associated with the $^4I_{9/2}(0) \rightarrow {}^2P_{1/2}$ transition at 23 539 cm^{-1}.

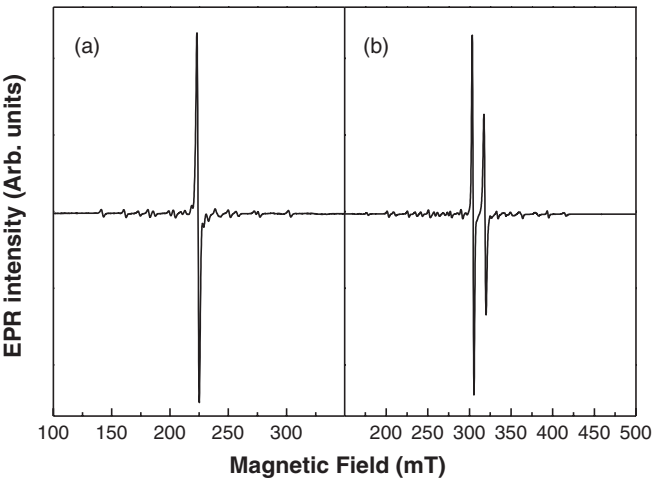

FIG. 6. Electron paramagnetic resonance spectra at 5 K for two different geometrical configurations: (a) Magnetic field in the (001) [or (ab)] plane and (b) magnetic field parallel to c axis.

P^k, is written as:

$$H_{\mathrm{FI}} = E_{\mathrm{ave}} + \sum_{k=2,4,6} f_k F^k + \zeta_{\mathrm{SO}} A_{\mathrm{SO}} + \alpha l(l+1) + \beta G(G_2) + \gamma G(R_7) + \sum_{i=2,3,4,6,7,8} T^i t_i + \sum_{j=0,2,4} M^j m_j + \sum_{k=2,4,6} P^k p_k. \quad (2)$$

It gives rise to 19 phenomenological parameters plus the mean energy of the whole configuration. A detailed description of the various operators and parameters is available in the literature.[23,24] At this point, it must be noted that some of the angular operators, namely t'_2, m_j, and p_k, have been recalculated to use a full orthogonal operator set[25] and to include the correction reported by previous authors.[26,27]

The even part of the one-electron CF Hamiltonian, responsible of the CF splitting, can also be written as a sum of products of the renormalized spherical tensor operators $[C_q{}^{(k)}]$,[28] and the real and imaginary parts of the CF parameters (B_q^k and $B_q'^k$, respectively):

$$H_{\mathrm{CF}}^{(\mathrm{even})} = \sum_{k,q} \boldsymbol{B}_q^k \left(C_q^{(k)}\right) = \sum_{k=2,4,6} B_0^k C_0^k + \sum_{q>0}^{\leqslant k} B_q^k \left[C_{-q}^{(k)} + (-1)^q C_q^{(k)}\right] + i B_q'^k \left[C_{-q}^{(k)} - (-1)^q C_q^{(k)}\right]. \quad (3)$$

The values of k and q, for which the parameters are nonzero, are determined by the local symmetry. For the C_S and C_2 symmetry, all the odd-q parameters vanish, and the CF Hamiltonian takes the form:[23]

$$\begin{aligned} H_{\mathrm{CF}}^{(\mathrm{even})}(C_s) = {} & B_0^2 C_0^{(2)} + B_2^2\left(C_{-2}^{(2)} + C_2^{(2)}\right) + i B_2'^2\left(C_{-2}^{(2)} - C_2^{(2)}\right) + B_0^4 C_0^{(4)} + B_2^4\left(C_{-2}^{(4)} + C_2^{(4)}\right) + i B_2'^4\left(C_{-2}^{(4)} - C_2^{(4)}\right) \\ & + B_4^4\left(C_{-4}^{(4)} + C_4^{(4)}\right) + i B_4'^4\left(C_{-4}^{(4)} - C_4^{(4)}\right) + B_0^6 C_0^{(4)} + B_2^6\left(C_{-2}^{(6)} + C_2^{(6)}\right) + i B_2'^6\left(C_{-2}^{(6)} - C_2^{(6)}\right) \\ & + B_4^6\left(C_{-4}^{(6)} + C_4^{(6)}\right) + i B_4'^6\left(C_{-4}^{(6)} - C_4^{(6)}\right) + B_6^6\left(C_{-6}^{(6)} + C_6^{(6)}\right) + i B_6'^6\left(C_{-6}^{(6)} - C_6^{(6)}\right), \end{aligned} \quad (4)$$

with 15 nonvanishing CF parameters (nine real and six imaginary).

In this highly nonlinear calculation, the starting values are crucial to yield a small root-mean-square (*rms*) deviation between the experimental and calculated energy levels, as well as to obtain consistent parameters. The initial estimations have been obtained making use of the very simplified simple overlap model (SOM).[29,30] It provides CF parameters given by:

$$B_q^k = \rho \left(\frac{2}{1 \pm \rho}\right)^{2k+1} \langle r^k \rangle A_q^k, \quad (5)$$

where ρ is the overlap between the metal and the ligand orbitals and the $\pm$ sign characterizes the displacement of the charge barycenter from the middle metal-ligand distance. The site symmetry of the rare earth ion is taken into account through the lattice sum A_q^k as:

$$A_q^k = \sqrt{\frac{4\pi}{2k+1}} \sum_j \frac{g_j}{R_j^{k+1}} Y_q^{k*}(j), \quad (6)$$

g_j being the charge of the ligands (F^- ions) and R_j its distance from the central Nd^{3+} ion and the radial integrals $\langle r^k \rangle$ (Freeman–Watson) values. Here, the reported structural data[18] with a value of $\rho = 0.08$ for the Nd^{3+} ion and overlapped orbitals (minus sign) has been used. Since there is no principal axis for the C_S symmetry, the quantization axis can be arbitrarily selected, and different sets of CF parameters (that could give the same CF splitting) can be obtained.[31,32] As starting CF parameters, we have selected those obtained with the quantization axis parallel to the crystallographic a axis [see Fig. 1(b)] with a suitable rotation around the quantization axis that makes the imaginary parameter $B'_2{}^2$ equal to zero.

D. Simulation procedure

Standard least-square methods were used to reproduce the electronic structure of the Nd^{3+} ion by means of an iterative fitting process that minimizes the *rms* value. The energy level analysis was carried out by using the complete $|SLJM\rangle$ basis set (182 Kramers doublets) for Nd^{3+} with a Hamiltonian with 19 free-ion parameters and 14 CF parameters. Since the number of levels empirically available for the present system is not large enough to support an analysis with such a large number of parameters, the simulation of the energy level structure of Nd^{3+} has been made in several steps.

The Nd^{3+} ^4I_J ($J = 9/2, \ldots, 15/2$) lowest multiplet is mainly pure. Thus, a first step in the CF analysis considers only the 26 ^4I_J Kramer's doublets in order to diagonalize the CF Hamiltonian in the Russell–Saunders coupling scheme. It also considers the ^4I_J barycenters as adjustable parameters and the full J-mixing effect. Since most of ^4I_J levels positions are experimentally obtained, this step should give a reasonable first approach to the CF parameters. However, several equivalent sets of CF parameters are obtained from this step. This ambiguity is associated with two facts. Firstly, the two-rank parameters are strongly related to the $^4F_{3/2}$ splitting. Secondly, in low symmetries, least squares fits are often unstable because the energy levels are relatively insensitive to the CF phase factor.[33]

The second step involves the use of the full Hamiltonian (free-ion plus CF) in the intermediate scheme with the complete $|SLJM\rangle$ basis set. Assuming that slight changes in the free-ion parameters do not significantly affect the behavior of CF parameters, we have used as starting free-ion parameters those calculated for Nd^{3+}:$LaCl_3$.[34]

As mentioned, the accurate determination of the free-ion Hamiltonian needs a large number of $^{2S+1}L_J$ multiplets, but due to the scarcity of experimental levels obtained by optical

TABLE I. Experimental and calculated energy level positions (in cm^{-1}) of the Nd^{3+} in BMF:Na^{+}.

$^{2S+1}L_J$ (degeneracy)	Experimental Stark energy levels	Calculated energy levels	Energy difference
$^4I_{9/2}$	0	2	0
	75	60	15
	417	247	170[a]
	425	429	4
	615	613	2
$^4I_{11/2}$	1978	1975	3
	2001	1998	3
	2097	2096	1
	2274	2275	1
	2303	2309	6
	2331	2335	4
$^4I_{13/2}$	3921	3921	0
	3932	3938	6
	4048	4050	2
	4236	4239	3
	4280	4279	1
	4310	4309	1
	4357	4365	8
$^4I_{15/2}$	5811	5816	5
	5896	5888	8
	6050	6042	8
	6227	6229	2
	6361	6360	1
		6439	
		6544	
		6617	
$^4F_{3/2}$	11 533	11 533	0
	11 770	11 761	9
$^4F_{5/2} + {}^2H(2)_{9/2}$		12 499	
	12 560	12 554	6
	12 621	12 632	11
	12 689	12 683	6
	12 770	12 768	2
		12 798	
		12 878	
		12 958	
$^4F_{7/2} + {}^4S_{3/2}$	13 487	13 527	40
	13 665	13 650	15
	13 753	13 722	32
	13 762	13 764	2
	13 784	13 785	1
	13 861	13 838	23
$^4F_{9/2}$		14 723	
	14 793	14 798	5
		14 946	
		15 045	
	15 060	15 076	16
$^2H(2)_{11/2}$		15 972	
		16 015	
		16 027	
		16 050	
		16 066	
		16 085	
$^4G_{5/2} + {}^4G_{7/2}$		17 167	
	17 292	17 309	17
		17 435	

TABLE I. (*Continued*.)

$^{2S+1}L_J$ (degeneracy)	Experimental Stark energy levels	Calculated energy levels	Energy difference
	17 470	17 472	2
	17 584	17 567	17
	17 644	17 648	4
	17 773	17 761	12
		19 150	
	19 174	19 174	0
		19 230	
	19 250	19 254	4
$^2K_{13/2} + {}^4G_{9/2}$	19 363	19 365	2
		19 443	
$^2K_{15/2} + {}^4G_{11/2}$		19 523	
		19 616	
$^2G(1)_{9/2} + {}^2D(1)_{3/2}$		19 667	
		19 767	
		19 810	
		19 880	
		19 966	
		19 986	
		20 113	
		20 341	
		21 001	
		21 048	
		21 075	
		21 105	
		21 172	
		21 327	
		21 387	
		21 432	
		21 534	
		21 567	
		21 637	
		21 686	
		21 734	
		21 780	
		21 897	
		21 980	
		22 020	
		22 087	
		22 139	
		22 164	
		22 431	
$^2P_{1/2}$	23 539	23 538	1
$^2D(1)_{5/2}$		23 729	
		24 008	
		24 172	
$^2P_{3/2}$		26 316	
		26 423	
$^4D_{3/2} + {}^4D_{5/2}$		28 205	
	28 334	28 342	8
	28 369	28 404	35
	28 769	28 768	1
	28 903	28 915	12
$^4D_{1/2}$	29 154	29 171	17
$^2I_{11/2}$		29 219	
		29 344	
		29 486	
		29 594	
		29 673	
		29 854	

[a]This energy level displays a bad fit and has been excluded from the calculation.

TABLE II. Atomic and CF parameters (in cm^{-1}) and obtained principal g values for Nd^{3+} in BMF:Na. The statistical uncertainties, given in parentheses, result from the complete fit of the free-ion and crystal-field parameters. Starting atomic parameters data ($LaCl_3$) were obtained from Ref. 34.*

	Atomic parameters		CF parameters		
	Initial ($LaCl_3$)	Best fit	Initial (SOM)		Best fit
E_{ave}		24508	B_0^2	493	716 (9)
F_2	71 866	73 239 (14)	B_2^2	791	724 (28)
F_4	52 132	52 448 (10)	B_0^4	− 371	− 375 (26)
F_6	35 473	35 197 (7)	B_2^4	366	778 (26)
α	22.08	22,26 (0.2)	$B'_2{}^4$	847	1338 (29)
β	− 650	− 611 (2)	B_4^4	− 59	− 414 (9)
γ	1586	1427 (6)	$B'_4{}^4$	− 81	− 270 (12)
T_2	377	291 (1)	B_0^6	− 1558	− 1213 (6)
T_3	40	49 (0)	B_2^6	375	280 (17)
T_4	63	67 (2)	$B'_2{}^6$	410	492 (10)
T_6	− 292	− 375 (2)	B_4^6	− 478	− 246 (35)
T_7	358	358 (0)	$B'_4{}^6$	24	204 (17)
T_8	354	354 (0)	B_6^6	− 273	− 585 (12)
ζ_{so}	880	866.9 (1.6)	$B'_6{}^6$	− 17	− 241 (62)
M_0	1.97	1.57 (0.5)			
P_2	255	471 (32)			
Crystal field strength			Principal g values		
S (cm^{-1})	621		$g_{\|\|} = g_{aa}$	2.95	
			$g_{\perp_1}$	1.26	
rms	18		$g_{\perp_2}$	2.56	

*$M^2/M^0 = 0.56$ and $M^4/M^0 = 0.38$. $P^4/P^2 = 0.75$ and $P^6/P^2 = 0.5$.

measurements (51), some restrictions in the number of variable atomic parameters are used in most steps of fitting procedure. Particular care was taken to avoid inconsistent values of T^i, M^j, and P^k.[35,36] In addition, a weighted function was used to include the experimental levels of most of the highest energy $^{2S+1}L_J$ multiplets.

The simulated energy levels are listed in Table I in comparison with the experimental ones. Table II reports the final set of atomic and CF parameters, which give the best fit to 50 experimental Kramer's doublets. For comparison purpose, the free-ion parameter values for $LaCl_3$ are also included.

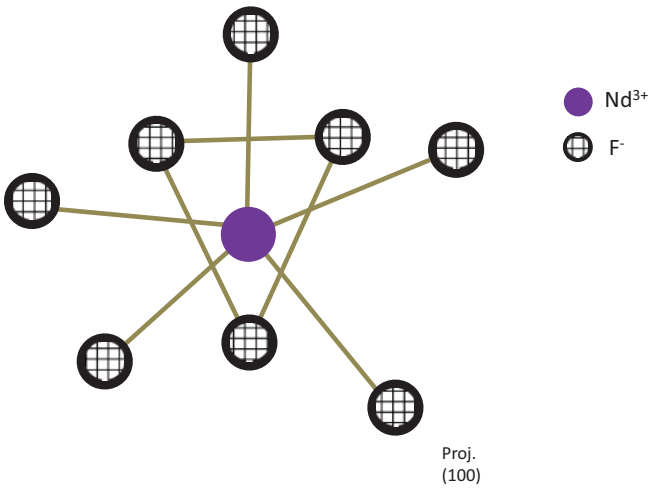

FIG. 7. (Color online) Suggested model for the Nd^{3+} environment in the Ba^{2+} site after the CF analysis. Projection along the a axis (100 projection).

The *rms* deviation for the final fit is 18 cm^{-1}, indicating a good agreement between the experimental and calculated Stark levels. The calculated total CF strength parameter S,[37] 621 cm^{-1}, is relatively strong, but considerably smaller than that for the cationic Mg^{2+} site. Therefore, the S value is consistent with the Ba^{2+} site location for Nd^{3+} ions in this fluoride host.

Table II also shows the obtained principal g values. They have been calculated by evaluating the matrix elements of the magnetic interaction, through the $L + g_e S$ tensor operator, as a perturbation operating on the ground state (Kramer's doublet) full eigenvectors.

Although the obtained fitting is very accurate, as indicated by the low *rms* value, it is worth noting that not all the CF parameters have been calculated with the same accuracy. Some of them may be varied in a wide range of values without giving rise to significant changes in the energetic positions of the calculated Stark levels. Indeed, some of the parameters have major influence in the calculation of the principal g values. Thus, some degree of uncertainty is expected in this calculation, mainly related with the g values perpendicular to the quantization axis (a crystallographic axis). In any case, a good agreement is observed between the experimental g values obtained by EPR and the theoretical ones obtained from our fitting, mostly considering the complexity of the problem: 14 crystal field parameters and only 50 energy levels.

We can tentatively relate the CF obtained in our fitting to the structural location of Nd^{3+} in BMF. The results point to a

distorted Ba^{2+} site in which the Nd^{3+} ion is shifted towards the center of the triangular prism [Fig. 1(b)] and a subsequent rearrangement of the five planar fluorine ligands. Therefore, the Nd^{3+} ions would locate in a more centrosymmetric configuration than that of regular Ba^{2+}sites, approaching a orthorhombic symmetry in agreement with the EPR results. The shift of Nd^{3+} ions would imply a reduction of the ferroelectric character of the host, which could be assessed in the case of very high dopant levels. The suggested model is schematically depicted in Fig. 7 in which an *a* view (100 projection) of the Nd^{3+} site is shown.

IV. CONCLUSION

The LT optical spectroscopy and EPR experiments confirm the single location of Nd^{3+} in the BMF:Na^{+} crystal. A CF analysis of Nd^{3+} ion has been carried out. The results show that the Nd^{3+} ion experiences a CF consistent with its incorporation into the Ba^{2+} site. It is suggested that Nd^{3+} distorts the Ba^{2+} regular site towards a more centrosymmetric location, which would approach an orthorhombic symmetry. The results shown provide basic information to understand the properties of trivalent rare earth-doped BMF Vacuum Ultraviolet-IR transparent crystal for potential optical devices.

ACKNOWLEDGMENTS

This work has been supported by the Spanish Ministry of Science under projects MAT2010-17443, MAT2010-21270-C04-02, Consolider-Ingenio MALTA CSD 2007-0045, and Comunidad Autónoma de Madrid under Grant 2009/MAT-1756.

*pablo.molina@uam.es

[1] K. T. Gahagan, V. Gopalan, J. M. Robinson, Q. X. Jia, T. E. Mitchell, M. J. Kawas, T. E. Schlesinger, and D. D. Stancil, Appl. Opt. **38**, 1186 (1999).
[2] W. R. Bosenberg, A. Drobshoff, J. I. Alexander, L. E. Myers, and R. L. Byer, Opt. Lett. **21**, 1336 (1996).
[3] N. G. R. Broderick, G. W. Ross, H. L. Offerhaus, D. J. Richardson, and D. C. Hanna, Phys. Rev. Lett. **84**, 4345 (2000).
[4] R. L. Byer, IEEE J. Sel. Top. Quantum Electron. **6**, 911 (2000).
[5] D. Jaque, J. Capmany, J. A. Sanz García, A. Brenier, G. Boulon, and J. García Solé, Opt. Mater. **13**, 147 (1999).
[6] E. Montoya, J. Capmany, L. E. Bausa, T. Kellner, A. Diening, and G. Huber, Appl. Phys. Lett. **74**, 3113 (1999).
[7] M. O. Ramírez, J. J. Romero, P. Molina, and L. E. Bausá, Appl. Phys. B **81**, 827 (2005).
[8] J. Capmany, Appl. Phys. Lett. **78**, 144 (2001).
[9] P. Molina, M. D. Ramirez, and L. E. Bausa, Adv. Funct. Mater. **18**, 709 (2008).
[10] M. O. Ramirez, D. Jaque, L. E. Bausa, J. Garcia Sole, and A. A. Kaminskii, Phys. Rev. Lett. **95**, 267401 (2005).
[11] E. G. Villora, P. Molina, S. Alvarez, J. V. Garcia-Santizo, M. O. Ramirez, K. Shimamura, and L. E. Bausa, J. Appl. Phys. **107**, 033106 (2010).
[12] E. G. Villora, K. Shimamura, F. Jing, A. Medvedev, S. Takekawa, and K. Kitamura, Appl. Phys. Lett. **90**, 192909 (2007).
[13] K. Shimamura, E. G. Víllora, K. Muramatsu, and N. Ichinose, J. Cryst. Growth **275**, 128 (2005).
[14] E. G. Víllora, K. Shimamura, K. Sumiya, and H. Ishibashi, Opt. Express **17**, 12362 (2009).
[15] V. Gopalan, V. Dierolf, and D. A. Scrymgeour, in *Annual Review of Materials Research* (Annual Reviews, Palo Alto, 2007), Vol. 37, p. 449.
[16] K. Recker, F. Wallrafen, and S. Haussühl, J. Cryst. Growth **26**, 97 (1974).
[17] K. Shimamura, E. G. Villora, H. Zeng, M. Nakamura, S. Takekawa, and K. Kitamura, Appl. Phys. Lett. **89**, 232911 (2006).
[18] F. Gingl, Z. Anorg. Allg. Chem. **623**, 705 (1997).
[19] M. Yamaga, K. Hattori, N. Kodama, N. Ishizawa, M. Honda, K. Shimamura, and T. Fukuda, J. Phys.: Condes. Matter **13**, 10811 (2001).
[20] S. Kuck, I. Sokolska, M. Henke, T. Scheffler, and E. Osiac, Phys. Rev. B **71**, 165112 (2005).
[21] J. V. Garcia-Santizo, B. del Rosal, M. O. Ramirez, L. E. Bausa, E. G. Villora, P. Molina, V. Vasyliev, and K. Shimamura, J. Appl. Phys. **110**, 063102 (2011).
[22] R. D. Shannon and C. T. Prewitt, Acta Crystallogr. Sec. B **25**, 925 (1969).
[23] C. Göller-Walrand and K. Binnemans, *Handbook on the Physics Chemistry of Rare Earths*, edited by K. A. Gschneidner Jr. and L. Eyring (North-Holland, Amsterdam, 1996).
[24] *Crystal Field Handbook*, edited by D. J. Newman and B. Ng (Cambridge University Press, Cambridge, 2000).
[25] J. E. Hansen, B. R. Judd, and H. Crosswhite, At. Data Nucl. Data Tables **62**, 1 (1996).
[26] B. R. Judd and E. Lo, J. Phys.: Condens. Matter **6**, L799 (1994).
[27] X. Chen, G. Liu, J. Margerie, and M. F. Reid, J. Lumin. **128**, 421 (2008).
[28] B. G. Wybourne, *Spectroscopic Properties of Rare Earths* (Wiley, New York, 1965).
[29] O. L. Malta, Chem. Phys. Lett. **87**, 27 (1982).
[30] O. L. Malta, Chem. Phys. Lett. **88**, 353 (1982).
[31] C. Rudowicz, J. Chem. Phys. **84**, 5045 (1986).
[32] C. Rudowicz and R. Bramley, J. Chem. Phys. **83**, 5192 (1985).
[33] G. W. Burdick and M. F. Reid, Mol. Phys. **102**, 1141 (2004).
[34] H. M. Crosswhite, H. Crosswhite, F. W. Kaseta, and R. Sarup, J. Chem. Phys. **64**, 1981 (1976).
[35] P. A. Tanner, V. Kumar, C. K. Jayasankar, and M. F. Reid, J. Alloy. Compd. **215**, 349 (1994).
[36] G. A. Kumar, R. E. Riman, A. A. Kaminskii, R. Praveena, C. K. Jayasankar, I. K. Bae, S. C. Chae, and Y. N. Jang, Phys. Rev. B **74**, 014306 (2006).
[37] N. C. Chang, J. B. Gruber, R. P. Leavitt, and C. A. Morrison, J. Chem. Phys. **76**, 3877 (1982).